# Novel statistically optimized one pot synthesis of inherently photoluminescent and electroactive graphene oxide nanosheets as 1, 4 dioxane sensor

R. Renjithkumar, B. Iffath, T. Devasena*
*Centre for Nanoscience and Technology, Anna University, Chennai-600025, Tamil Nadu, India*

1, 4 dioxane predominantly found in industrial effluents and air force plants, is of great concern worldwide due to its toxic and carcinogenic nature. Currently, there are limited research on 1,4 dioxane sensors and most of these sensors are intricate metal oxide composites. This study reports the fabrication of novel inherently electroactive graphene oxide nanosheets derived from a natural polyphenolic compound, and the process parameters were statistically optimized using TOPSIS based Taguchi $L_9$ orthogonal array. The proposed novel sensor was employed in the linear range (0.1µM to 3µM) that conforms with the WHO guideline (0.56 µM) for dioxane in water, showed good sensitivity (117 $nAnM^{-1}cm^{-2}$), detection limit (20.51 nM) and quantification limit (62.16 nM) which is far superior compared to the reported literature on dioxane sensing systems.

(Received December 8, 2022; Accepted March 13, 2023)

*Keywords:* Graphene oxide, Curcumin, 1,4 dioxane, TOPSIS-based Taguchi approach, Electrochemical sensor

## 1. Introduction

1,4 Dioxane ($C_4H_8O_2$) is a nonbiodegradable heterocyclic diether that is used as solvent in various industrial processes and also as an additive in automotive fluids, antifreeze and aircraft deicing processes [1]. Due to its high solubility in water and high volatility, it is prone to polluting water resources and contaminating the environment [2]. The US Environmental Protection Agency has classed it as a toxic chemical, a hazardous pollutant, and a class 2B carcinogen [3,4]. In conjunction, 1,4-dioxane is neurotoxic and is also accountable for various organ failures in humans [5]. This necessitates for the development of highly sensitive and reliable detection of 1,4 dioxane in aqueous media, for which electrochemical sensing is the most promising approach.

In the last decade, graphene oxide-based electrochemical sensors have attracted considerable interest due to their abundant oxygen containing functional groups that accords extraordinary electrocatalytic properties particularly for the oxidation of organic molecules [6-10]. There are several reports on the synthesis of GO by various methods using graphite as the carbon source [11], however, GO synthesized from graphite exhibits low electrical conductivity [12]. In order to overcome this problem, GO conjugated with polymer and metal nanocomposites have been reported for the enhanced electrochemical sensing of various target analytes thitherto [12,13]. To the best of our knowledge, this is the first report on bare GO being employed for the electrochemical detection of an analyte. The present work has focused on fabricating a simple metal free catalyst as the electrode material that has excellent current response to 1, 4 dioxane with high specificity, sensitivity, reproducibility and stability. To achieve this, GO was synthesized from a natural phytochemical named curcumin ($C_{21}H_{20}O_6$), the active principle of turmeric, that exhibits intrinsic electrocatalytic properties and is reported to have specificity towards dioxane [14]. As the proposed work involves a novel method of GO synthesis, process optimization becomes the essential part of the study. For this purpose, TOPSIS (Technique for Order Preference by Similarity to an Ideal Solution) based Taguchi $L_9$ orthogonal array approach was used for optimizing the synthesis process parameters [15]. The application of the TOPSIS-based Taguchi

* Corresponding author: tdevasenabio@gmail.com
https://doi.org/10.15251/DJNB.2023.181.377

method does not require complex mathematical tools and is appropriate for multi-variable optimization problems [16,17].

This novel approach of GO synthesis from curcumin as the carbon source possesses several advantages over the currently existing methods of GO synthesis that involve reactions of graphite with strong oxidants, posing an explosion risk, serious environmental pollution and long-reaction time. In addition to this, the GO obtained by this method is inherently photoluminescent and electroactive in nature, which could be deployed in various optical and electrochemical applications. In this study, this novel GO was utilized for the electrochemical detection of 1,4 dioxane owing to its intrinsically unique properties.

## 2. Experimental

### 2.1. Materials

1,4-Dioxane ($C_4H_8O_2$, 99%), potassium hexacyanoferrate ($K_3FeCN_6$), acetone, DMF (Dimethylformamide), DMSO (Dimethyl sulfoxide) and curcumin ($C_{21}H_{20}O_6$) were obtained from SRL Pvt. Ltd. Nafion solution was purchased from Sigma Aldrich. All the chemicals used in this study were of analytical grade. The electrochemical analysis experiments were performed in 0.1M PBS (pH 7.0) as the electrolyte. All the solutions for electrochemical characterizations were made using Millipore deionized (DI) water (18.2 MΩ cm @ 25 °C) and the studies were carried out at ambient temperatures.

### 2.2. Graphene oxide synthesis from curcumin

Four samples of 25 mg/ml concentration curcumin solution were prepared by dissolving curcumin in acetone, DMF, DMSO and water respectively. The solvents were chosen based on their polarity indices and the solubility of curcumin in these solvents (curcumin is highly soluble in acetone and insoluble in water) [18]. The preliminary test for graphene oxide (GO) synthesis was performed by pyrolyzing the above 4 solutions in triplicates for 15 mins at temperatures above the degradation temperature of curcumin (180$^o$C) [19]. It was observed that curcumin was converted to graphene oxide at the pyrolysis temperature of 300 $^0$C, with acetone as the oxidizing agent.

### 2.2. Optimization of synthesis process parameters

The first step of this study is to identify three performance criteria (ID/IG ratio, I2D and ID+D' that corresponds to the $sp^2$ carbon domains, disorder and defects in the GO structure respectively [15,20] along with three factors (temperature, time and precursor concentration) having three control levels (chosen based on the preliminary test result), for the Taguchi based design of experiments (table 1). In order to analyze the factor effects, a Taguchi orthogonal array $L_9$ ($3^3$) was constructed to record the experimental results (table 2). Based on this array, triplicates of 9 samples (S1 to S9) were prepared and characterized by Raman spectroscopy (Agiltron Inc. Peak seaker Pro 532). The excitation wavelength and the excitation laser energy were selected as 532 nm and 10 mV, respectively. The Raman spectra of the 9 samples exhibited a G-band at 1590 $cm^{-1}$, D band at 1350 $cm^{-1}$, 2D at 2700 $cm^{-1}$ and D+D' band at 2930 $cm^{-1}$ with slight differences in position and relative intensity. The obtained ID/IG, I2D and I(D + D') values of each experimental run are given in table 3, which demonstrates the successful conversion of curcumin to graphene oxide for the samples from S1 to S6. From S7 to S9, an increase in ID/IG ratios was observed, which could be due to the formation of new and smaller $sp^2$ domains, thus indicating the reduction of the oxidized product (GO) towards reduced graphene oxide (rGO). The results of the Raman spectroscopy are displayed in Fig.1.

The multi-response was then converted to single-response by using TOPSIS methodology steps such as calculation of the decision matrix, weighted normalized decision matrix, identification of positive ideal and negative ideal solutions ($A^+$ and $A^-$), calculation of the separation measures ($S_i^+$ and $S_i^-$) and calculation of the ranking scores or relative closeness ($C^*$) for GO (table 4) using the standard formulae as per the literature [15,20,21]. The values of the decision matrix (table 4) for R1 (ID/IG), R2 (I2D) and R3 (ID+D') were calculated to be 2.11, 68.24, 64.79 respectively. The positive ideal ($A^+$) for ID/IG, I2D and ID+D' were calculated to be

0.244, 0.143 and 0.007 respectively. The negative ideal solutions ($A^-$) for ID/IG, I2D and ID+D' were calculated to be -0.057, 0.010 and -0.148 respectively. It could be observed from Table 4 that S4 was ranked 1, and also, table 5 shows largest delta value (δ) for temperature (A) followed by time (B) and concentration (C). Thus, it could be concluded that the temperature is the most influencing factor for GO synthesis by this method. Thus, from the SN graph shown in table 5, the optimum process parameters obtained from TOPSIS based Taguchi design of experiments for GO synthesis was found to be $A_2B_1C_2$.

*Table 1. Performance criteria, factors and their levels.*

| Performance criteria | Factors | Symbol | Levels | | |
|---|---|---|---|---|---|
| | | | 1 | 2 | 3 |
| ID/IG | Temperature ($^oC$) | A | 300 | 400 | 500 |
| I2D | Time (min) | B | 10 | 20 | 30 |
| I(D+D') | Concentration (mg/ml) | C | 50 | 25 | 16.67 |

*Table 2: $L_9$ ($3^3$) Taguchi orthogonal array design.*

| Exp. No. | Coded levels | | | Uncoded levels | | |
|---|---|---|---|---|---|---|
| | A | B | C | A | B | C |
| S 1 | 1 | 1 | 1 | 300 | 10 | 50 |
| S 2 | 1 | 2 | 2 | 300 | 20 | 25 |
| S 3 | 1 | 3 | 3 | 300 | 30 | 16.67 |
| S 4 | 2 | 1 | 2 | 400 | 10 | 25 |
| S 5 | 2 | 2 | 3 | 400 | 20 | 16.67 |
| S 6 | 2 | 3 | 1 | 400 | 30 | 50 |
| S 7 | 3 | 1 | 3 | 500 | 10 | 16.67 |
| S 8 | 3 | 2 | 1 | 500 | 20 | 50 |
| S 9 | 3 | 3 | 2 | 500 | 30 | 25 |

*Table 3. Response values for GO obtained by $L_9$ Taguchi orthogonal array design.*

| Exp | ID/IG ratio | | | | I2D values | | | | ID+D' values | | | |
|---|---|---|---|---|---|---|---|---|---|---|---|---|
| | R1 | R2 | R3 | Mean | R1 | R2 | R3 | Mean | R1 | R2 | R3 | Mean |
| S 1 | 0.9 | 0.91 | 0.92 | 0.91 | 2.79 | 3.78 | 1.8 | 2.7 | 1.2 | 5.3 | 3.28 | 3.28 |
| S 2 | 0.95 | 0.96 | 0.97 | 0.96 | 27.4 | 30 | 31.9 | 29.7 | 23.7 | 21.5 | 25.9 | 23.7 |
| S 3 | 0.97 | 0.96 | 0.97 | 0.97 | 15.2 | 19.7 | 24.2 | 19.7 | 15 | 18.1 | 12 | 15 |
| S 4 | 0.85 | 0.81 | 0.83 | 0.83 | 1.19 | 1.2 | 1.3 | 1.2 | 1.17 | 1.1 | 1.2 | 1.17 |
| S 5 | 0.87 | 0.89 | 0.88 | 0.88 | 16.5 | 20.8 | 18.8 | 18.7 | 21.3 | 21.5 | 21.2 | 21.3 |
| S 6 | 0.99 | 0.98 | 1.01 | 0.99 | 18.2 | 24.6 | 12.0 | 18.2 | 9.25 | 9.12 | 12.2 | 10.1 |
| S 7 | 1.01 | 1.02 | 1.01 | 1.01 | 25.2 | 23.3 | 27.2 | 25.2 | 25.9 | 23.7 | 27.8 | 24.8 |
| S 8 | 1.01 | 1.03 | 1.06 | 1.03 | 27.7 | 26.8 | 24.9 | 26.5 | 27.8 | 29.6 | 26.0 | 27.8 |
| S 9 | 1.04 | 1.04 | 1.04 | 1.04 | 4.15 | 4.78 | 3.54 | 4.15 | 2.21 | 2.28 | 2.34 | 2.28 |

*Table 4. Multiresponse optimization for GO using TOPSIS L9 (33) Taguchi Design.*

| Exp | Decision matrix (S/N ratios) | | | Weighted normalized decision matrix | | | SEPARATION MEASURES | | SCORE | RANK |
|---|---|---|---|---|---|---|---|---|---|---|
| | R1 | R2 | R3 | $v_{i1}$ | $v_{i2}$ | $v_{i3}$ | $S_i^+$ | $S_i^-$ | $C_i^*$ | |
| S 1 | 0.76 | 8.91 | -10.31 | 0.119 | 0.04 | -0.053 | 0.16 | 0.16 | 0.55 | 3 |
| S 2 | 0.31 | 29.48 | -27.51 | 0.050 | 0.14 | -0.141 | 0.23 | 0.23 | 0.42 | 4 |
| S 3 | 0.26 | 25.89 | -23.55 | 0.041 | 0.12 | -0.121 | 0.23 | 0.23 | 0.39 | 5 |
| S 4 | 1.55 | 2.07 | -1.36 | 0.244 | 0.01 | -0.007 | 0.13 | 0.13 | 0.71 | 1 |
| S 5 | 1.03 | 25.44 | -26.6 | 0.162 | 0.12 | -0.136 | 0.15 | 0.15 | 0.61 | 2 |
| S 6 | 0.04 | 25.21 | -20.14 | 0.006 | 0.12 | -0.103 | 0.25 | 0.25 | 0.34 | 6 |
| S 7 | -0.16 | 28.04 | -27.91 | -0.025 | 0.13 | -0.143 | 0.30 | 0.30 | 0.30 | 7 |
| S 8 | -0.29 | 28.47 | -28.89 | -0.046 | 0.13 | -0.148 | 0.32 | 0.32 | 0.28 | 8 |
| S 9 | -0.36 | 12.36 | -7.15 | -0.057 | 0.06 | -0.036 | 0.31 | 0.31 | 0.28 | 9 |

*Table 5. Main effects plot for SN ratios of optimized GO.*

| Level | Response Table for Signal to Noise Ratios | | |
|---|---|---|---|
| | A | B | C |
| 1 | -6.892 | -6.175 | -7.535 |
| 2 | -5.437 | -7.546 | -7.167 |
| 3 | -10.789 | -9.398 | -8.416 |
| δ | 5.352 | 3.223 | 1.249 |
| Rank | 1 | 2 | 3 |

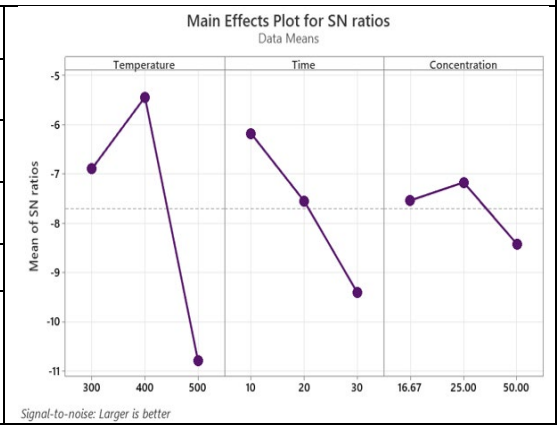

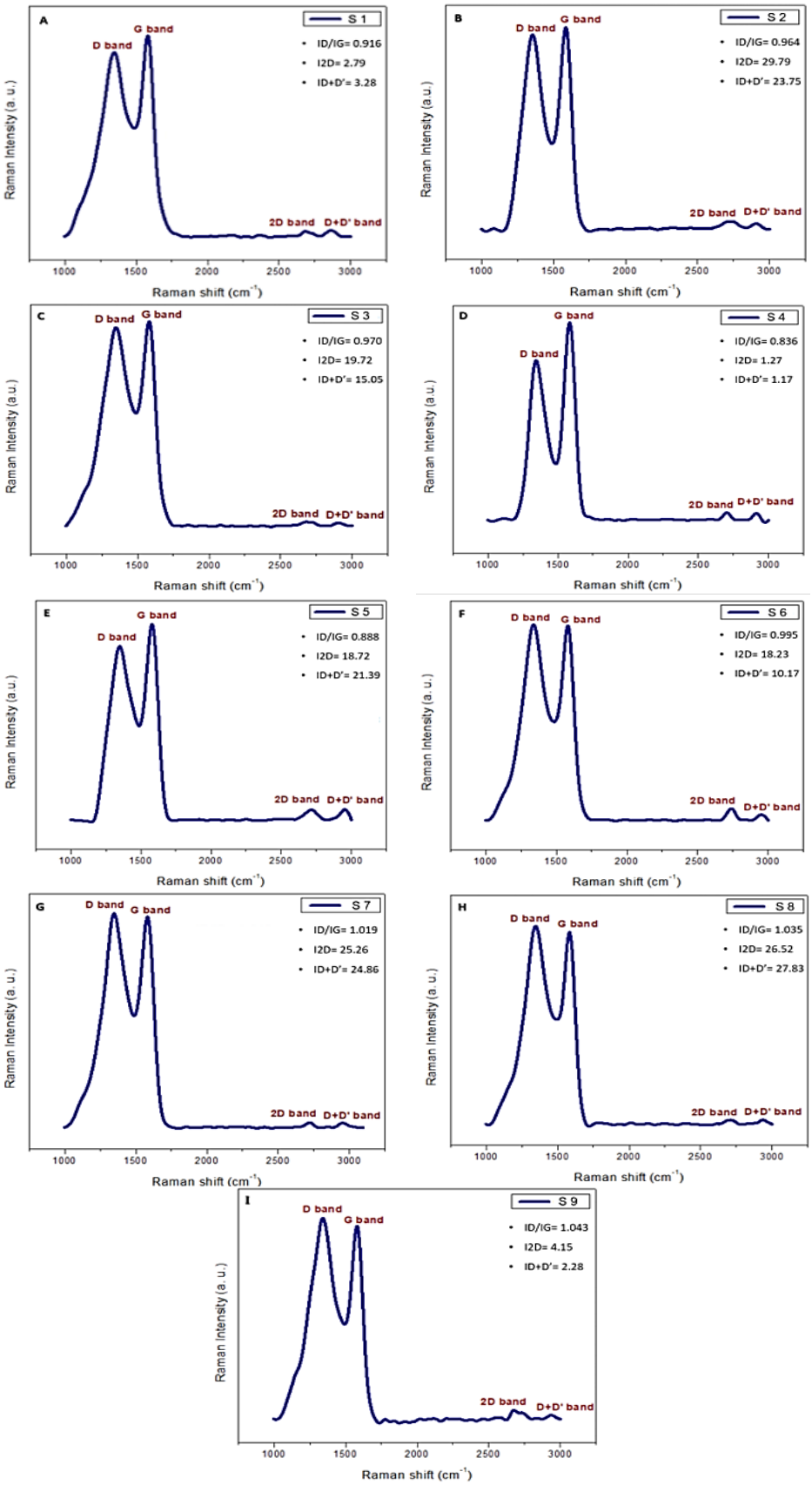


*Fig. 1. Raman spectroscopy of GO synthesized by Taguchi $L_9$ ($3^3$) design.*

## 3. Results and discussion

### 3.1. Physical characterization of GO

In order to confirm the formation of GO from curcumin, the synthesized sample was characterized for its physical, optical and electrochemical properties. The observations of the FTIR spectroscopy (Jasco International Company Ltd, 6600) of the sample shown in Fig. 2(b) were in excellent accordance with the previously published reports on GO [22-24]. The O-H stretching and bending vibrations of GO are attributable to the wide and intense peaks at 3405 $cm^{-1}$ and 1403 $cm^{-1}$. The hydrogen bound OH groups of dimeric COOH groups are responsible for a minor peak at 2926 $cm^{-1}$, and the intra-molecular O-H stretching of alcoholic group is responsible for a smaller peak at 2849 $cm^{-1}$, as illustrated in Fig. 2. The peak at 1624 $cm^{-1}$ is attributed to C=C stretching. The C=O stretching vibration of –COOH groups found in the graphene oxide nanosheets was observed at 1727 $cm^{-1}$ [25]. Thus, the synthesized sample did not show peaks pertaining to curcumin (fig 2(a)) and showed the presence of characteristic peaks corresponding to GO, thereby confirming the transformation of curcumin to graphene oxide. Further, the XRD (Rigaku Miniflex 600) pattern of GO shown in fig 3(a) exhibits diffraction peaks at $11.5^0$ and $41.4^0$, corresponding to 002 and 100 planes respectively, that further confirms the presence of GO [24]. Fig 3(b) shows the SEM (Tescan, Vega.3.SBU) images of the optimized GO taken at 30kV, 10kx magnification and 2µm resolution, which shows sheet like structures stacked as layers in nanoscale confirming that the above synthesized GO exhibits the morphology of nanosheets.

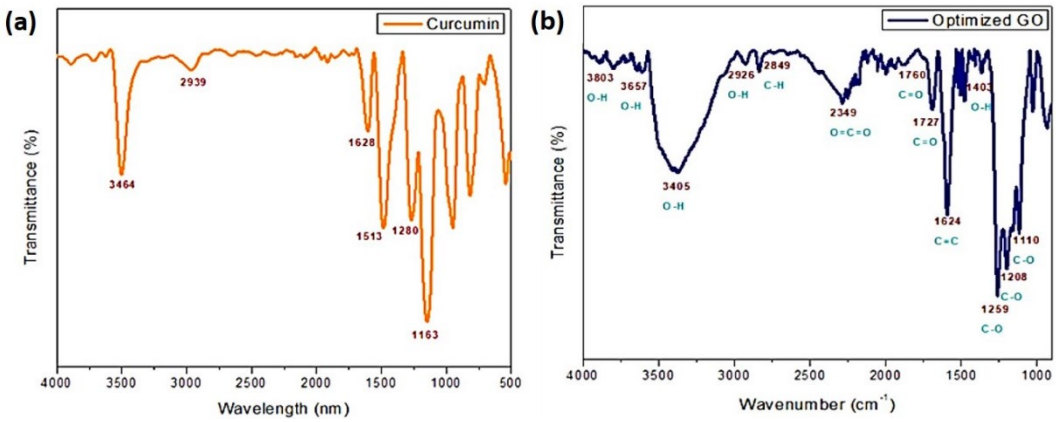


*Fig. 2. FTIR spectra of (a) Curcumin (b) Optimized GO.*

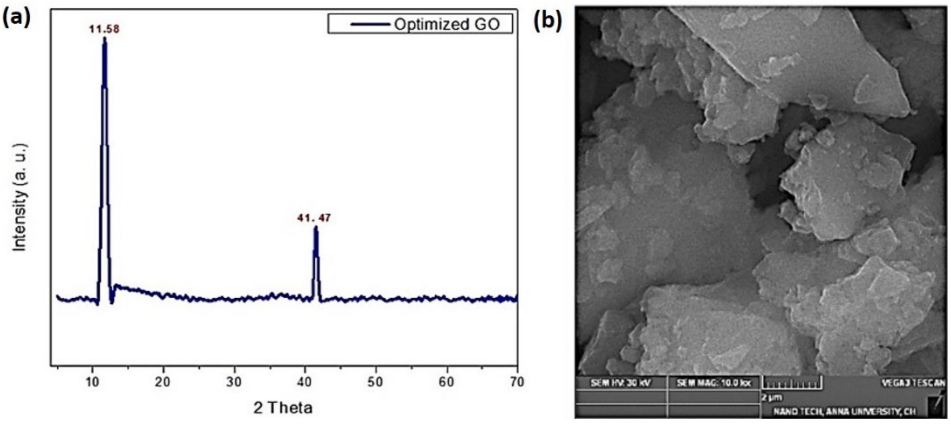


*Fig. 3. (a) XRD pattern of optimized GO. (b) SEM image of optimized GO.*

### 3.2. Optical characterization of GO

The results of UV-absorption spectroscopy (T90+ PG INSTRUMENTS) shown in fig 4(b) exhibit a maximum absorption peak at 225 nm that corresponds to π-π* transition of aromatic C-C bonds and a shoulder peak at 280 nm which corresponds to n-π* transition of C=O which are in accordance with the previously reported studies on GO [24, 26]. The oxidation of curcumin causes the generation of C-C bonds of the aromatic class, which reflect the abundance and distribution of C-C bonds in GO. Additionally, a higher absorbance value of the shoulder peak indicates the prevalence of n-π* transition of the carbonyl groups, as per the literature [26]. The UV absorption spectrum of curcumin is shown in fig 4(a). Hence, it is evident that the obtained GO from curcumin contains comparatively higher number of aromatic C-C groups and carbonyl bonds than GO obtained from graphite source. The optical bandgap energy of GO calculated using Tauc plot equation (fig 5(a)) was found to be 4.8 eV which is 2.18 times higher than the optical bandgap of GO obtained by conventional methods which is around 2.2 eV [27]. The photoluminescence measurement was done by exciting the sample using a xenon lamp, and the typical excitation intensity used was ~2.8 mW/cm$^2$. The emitted photons were detected using a charged coupled device spectrometer. This GO from curcumin exhibits enhanced photoluminescence showing emission around 450 nm that corresponds to the blue region of the electromagnetic spectrum as shown in fig 5(b), which is probably due to its increased number of oxygen containing functional groups.

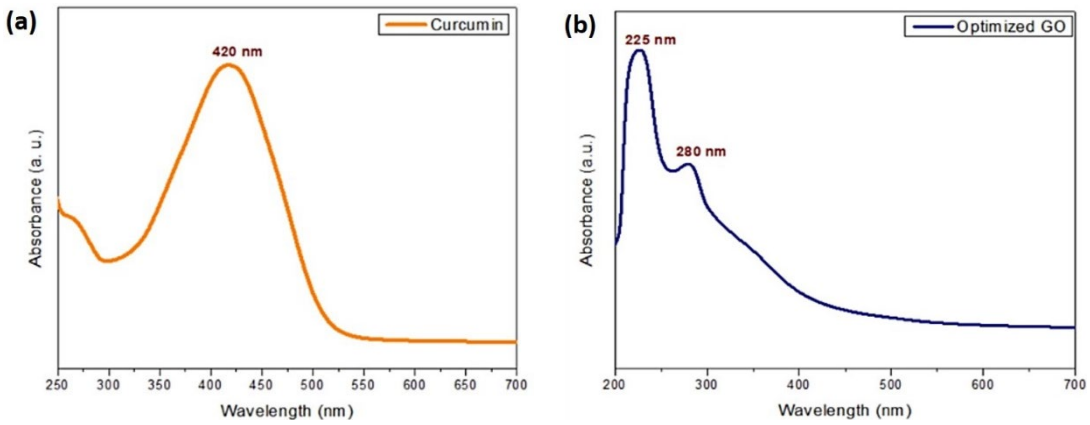


*Fig. 4. UV-Visible spectroscopy of (a) Curcumin. (b) GO.*

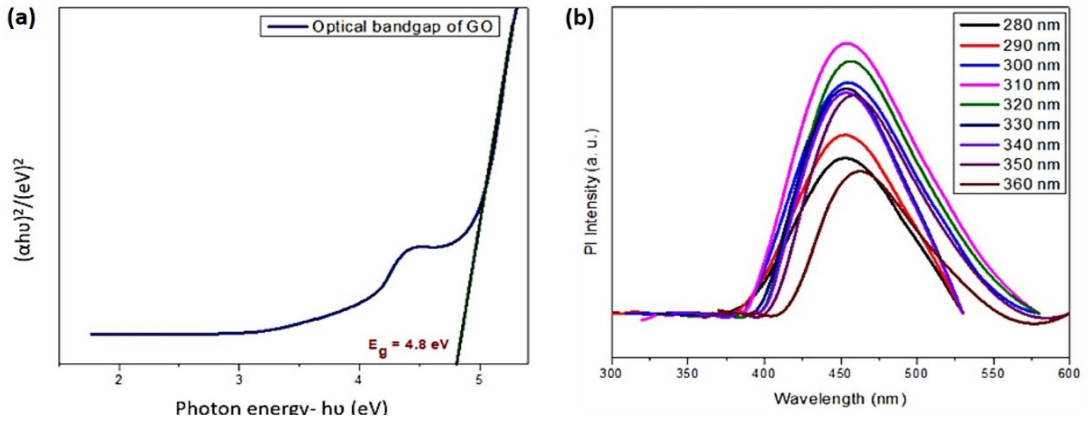


*Fig. 5. (a) Optical bandgap energy of GO. (b) PL spectroscopy of GO.*

### 3.3. Electrochemical characterization of GO

The electrochemical impedance measurement was made by dipping the bare GCE and GO modified GCE in 0.1 M PBS solution containing 5 mM $K_3FeCN_6$ in a frequency range from 10

mHz to 100 KHz. Fig 6(a) shows the variations in faradic impedance for the modified and bare electrode. From the absence of semicircle in the high frequency region of the EIS plot, it is evident that the GO modified electrode exhibits low charge transfer resistance at the electrode-electrolyte interface. The cyclic voltametric response of the GO modified electrode was measured and compared with bare electrode by performing CV experiment in 0.1M PBS solution (pH 7), at the scan rate of 50 $mVs^{-1}$. The cyclic voltammograms are shown in fig 6(b), from which it could be inferred that the anodic (oxidation) peak current (Epa) and the cathodic (reduction) peak current ($E_{pc}$) for GO modified GCE is at 0.58V and -0.002V respectively, whereas, there is no significant oxidation or reduction peak observed for bare GCE. Thus, the low charge transfer resistance obtained from EIS and the greater current response of CV clearly indicate the efficiency of novel GO to serve as a good electrode material.

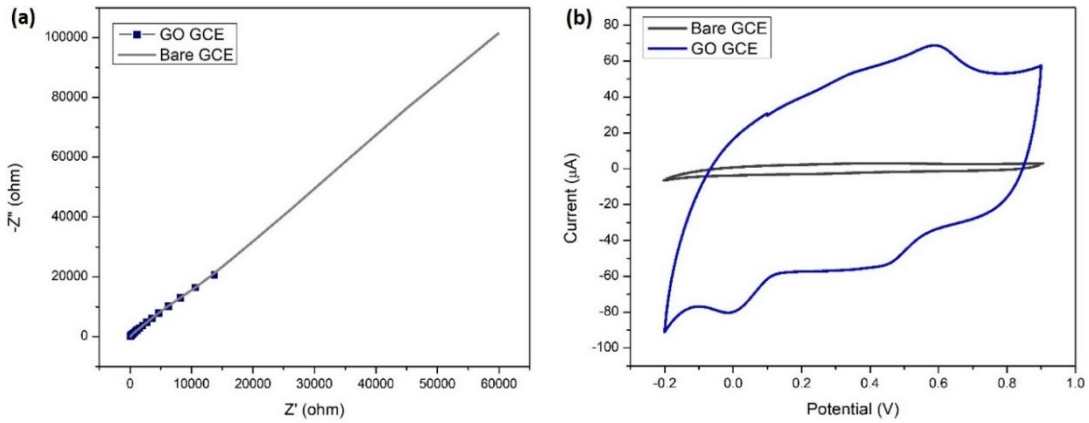


*Fig. 6. (a) Electrochemical impedance spectra of GO modified GCE and bare GCE. (b) Cyclic voltametric response of GO modified GCE and bare GCE.*

### 3.4. Electrochemical sensing performance of GO towards 1,4 dioxane

#### *3.4.1. Sensitivity of the novel GO modified electrode*

The sensitivity of the GO modified electrode towards 1,4 dioxane (3 µM in 0.1M PBS) was assessed by using LSV technique (50 mV/s scan rate; potential range: 0 to +1.5 V). Fig 7 shows that the anodic peak current for GO modified electrode was obtained at 0.58V, in contrast to the bare electrode. Fig 8(a) shows the sensitivity of the GO GCE towards different concentrations of 1,4 dioxane (0.1 µM to 3 µM) in 30 ml of 0.1M PBS solution (pH 7). From the current response obtained for every rise in the concentration of dioxane, it could be observed that in the absence of dioxane, the anodic (oxidation) peak appears at 0.58 V, but with the addition of analyte (0.1 µM 1,4 dioxane), a new small peak is observed at 0.78V. As the dioxane concentration increases from 0.1 µM to 3 µM a steady rise in current at 0.78V was also observed. The corresponding calibration curve, plotted with the obtained peak current (µA) versus the concentration (nM), is illustrated in Fig 8(b). The linear regression equation was calculated as I(µA)= 0.0083x(nM)+19.996 with $R^2$=0.99. The limit of detection (LOD), limit of quantification (LOQ) and sensitivity for the linear range 0.1 µM to 3 µM were calculated to be 20.51 nM, 62.16 nM and 117 nA $nM^{-1}$ $cm^{-2}$ as per the standard formulae mentioned in the literature [14, 28].

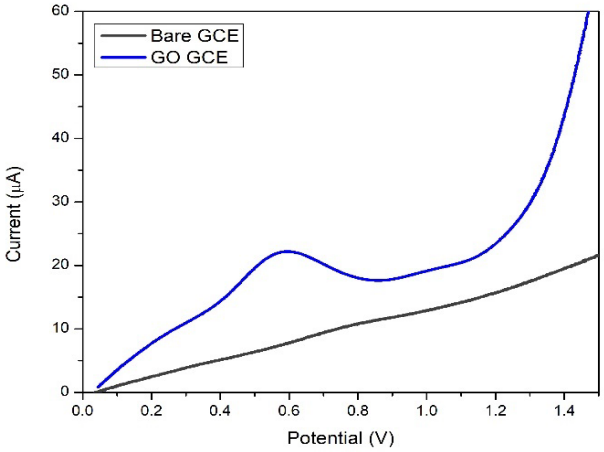


*Fig. 7. Linear sweep voltammograms of GO modified GCE and bare GCE.*

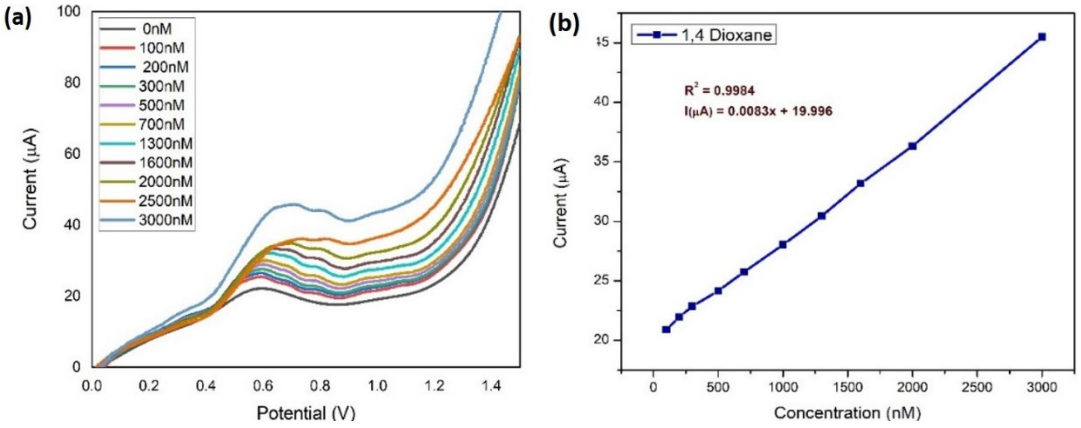


*Fig. 8. Linear sweep voltammograms of GO/GCE for 0.1μM to 3μM concentrations of 1,4 dioxane. (b) Corresponding linear plot of anodic peak current versus various concentrations of 1,4 dioxane.*

*3.4.1.1. Possible sensing mechanism*

The electrochemical detection mechanism of 1,4-dioxane is summarized in fig 10. On the surface of the novel GO modified electrode, 1,4-dioxane gets converted to formic acid and oxalic acid with the release of an electron which in turn increases the conductivity of the fabricated electrode. As a result, the electrochemical response increases with increase in the concentration of 1,4 dioxane. In addition to this, the greater number of active sites and oxygen containing functional groups of the novel GO enhance the sensing performance of the proposed sensor.

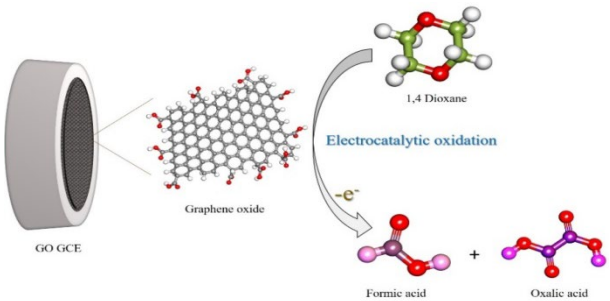


*Fig. 9. Electrochemical sensing mechanism of GO GCE towards 1,4 dioxane.*

### *3.4.2. Specificity, reliability and stability of the novel GO sensor*

The specificity of the novel GO sensor towards 1,4 dioxane was assessed by using LSV experiment carried out with 3 µM 1,4 dioxane in 0.1M PBS (pH 7), 0-1V potential window and 50 V/s scan rate with 1mM concentration of three interferents such as acetonitrile, chlorobenzene and ethylene glycol. From fig. 10, the significant difference in the oxidation potential between 1,4 dioxane and other interferents could be observed. Thus, it could be concluded that the proposed novel sensor has good specificity towards 1,4 dioxane. The reliability of the proposed novel sensor was evaluated by continuously running 35 LSV runs in 2µM dioxane in 30ml 0.1M PBS. From fig 11(a), it could be observed that, for the first 24 runs, there is no significant change in the peak current (RSD= 0.81%). After 25$^{th}$ run, linear decrease in current response for each run was observed. The stability of the proposed novel sensor was tested by measuring the peak current of the novel GO GCE in 2µM dioxane in 30ml 0.1M PBS for 14 days continuously. From fig 11(b), no significant change in the peak current (RSD= 0.47%) was observed for the first 10 days, however after which, a linear decrease in the anodic peak current was observed. This confirms that the proposed novel GO sensor shows good reliability and stability.

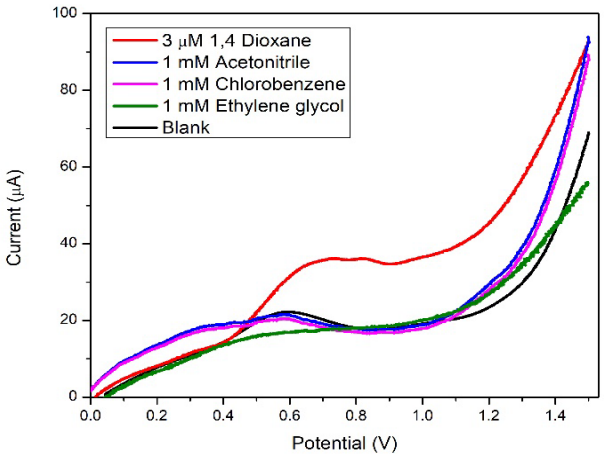


*Fig. 10. Specificity of novel GO towards 1,4 dioxane.*

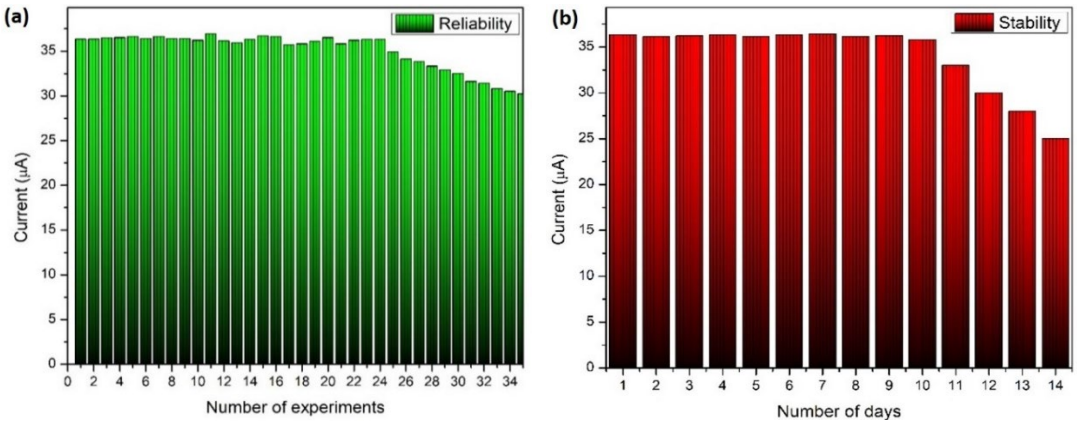


*Fig. 11. (a) Reliability of the proposed novel GO sensor. (b) Stability of the proposed novel GO sensor.*

## 4. Conclusion

Overall, we have successfully formulated the synthesis and process optimization of novel inherently photoluminescent and electroactive graphene oxide nanosheets from curcumin as the precursor. The synthesis process parameters were statistically optimized using TOPSIS based Taguchi $L_9$ orthogonal array. In this approach, three performance criteria were identified for the GO synthesis in which three factors having three control levels were chosen. A decision matrix was generated from the S/N ratios calculated for all the responses by running scenarios that combine factor levels in Taguchi design. The multi-response was then transformed to single response by TOPSIS method.

The optimized GO was then characterized for its physical, optical and electrochemical properties. The novel GO modified electrode showed a remarkable enhancement in the electrochemical performance towards 1,4 dioxane with good specificity and sensitivity of 117 $nAnM^{-1}cm^{-2}$ in the linear range (0.1µM to 3µM) that conforms with the WHO guideline (0.56 µM) for dioxane in water. The proposed sensor also showed detection limit of 20.51 nM and quantification limit of 62.16 nM, with good reliability and stability. Thus, this study reports the efficiency of novel GO as an excellent electrode material for the electrochemical sensing of 1, 4 dioxane in water.

## References

[1] K. G. Mohr Thomas, H. W. DiGuiseppi, J. K Anderson, J. W Hatton, 2nd ed. Boca Raton, CRC Press, 549 (2020); https://doi.org/10.1201/9780429401428
[2] X. Guan, F. Liu, J. Wang, C. Li, X. Zheng, Water Science and Technology **77**(1), 123 (2018); https://doi.org/10.2166/wst.2017.498
[3] H. M. Coleman, V. Vimonses, G. Leslie, R. Amal, Journal of Hazardous Materials **146**(3), 496 (2007); https://doi.org/10.1016/j.jhazmat.2007.04.049
[4] A. Kumar, G. Vyas, M. Bhatt, S. Bhatt, P. Paul, Chemical Communications **51**(88), 15936 (2015).
[5] M. M. Rahman, M. M. Alam, A. M. Asiri, RSC advances **9**(72), 42050 (2019); https://doi.org/10.1039/C9RA09118A
[6] M. Coros, F. Pogacean, L. Magerusan, C. Socaci, S. Pruneanu, Frontiers of Material Science **13**(1), 23 (2019); https://doi.org/10.1007/s11706-019-0452-5
[7] S. Rao, J. Upadhyay, K. Polychronopoulou, R. Umer, R. Das, Journal of Composites Science **2**(2), 25 (2018); https://doi.org/10.3390/jcs2020025
[8] Z. Zhang, H. C. Schniepp, D. H. Adamson, Carbon **154**, 510 (2019); https://doi.org/10.1016/j.carbon.2019.07.103
[9] P. D. Priya Swetha, H. Manisha, K. Sudhakaraprasad, Particle and Particle Systems Characterization **35**(8), 1800105 (2018); https://doi.org/ 10.1002/ppsc.201800105
[10] T. Devasena, B. Iffath, R. Renjith Kumar, N. Muninathan, K. Baskaran, T. Srinivasan, S. T. John, Bioinorganic Chemistry and Applications **2022**(2), 1-21 (2022); https://doi.org/10.1155/2022/4348149
[11] L. Sun, Chinese Journal of Chemical Engineering **27**(10), 2251 (2019); https://doi.org/10.1016/j.cjche.2019.05.003
[12] L. Qian, A. R. Thiruppathi, R. Elmahdy, J. Van der Zalm, A. Chen, Sensors **20**(5), 1252 (2020); https://doi.org/10.3390/s20051252
[13] Q. Zeng, H. Dong, X. Wang, T. Yu, W. Cui, Journal of hazardous materials **331**, 88 (2017); https://doi.org/10.1016/j.jhazmat.2017.01.040
[14] T. K. Sana Fathima, A. Banu, T. Devasena, S. Ramaprabhu, RSC advances **12**(30), 19375 (2022).
[15] B. Simsek, T. Yusuf, E. H. Simsek, Chemometrics and Intelligent Laboratory Systems. **125,** 18-32 (2013); https://doi.org/10.1016/j.chemolab.2013.03.012
[16] Y. Kuo, T. Yang, G. W. Huang, Engineering Optimization **40**(6), 517 (2008); https://doi.org/10.1080/03052150701857645

[17] T. Yang, P. Chou, Mathematics and Computers in Simulation **68**(1), 9 (2005); https://doi.org/10.1016/j.matcom.2004.09.004
[18] K. I. Priyadarsini, Molecules **19**(12), 20091 (2014); https://doi.org/10.3390/molecules191220091
[19] T. Esatbeyoglu, K. Ulbrich, C. Rehberg, S. Rohn, G. Rimbach, Food & function **6**(3), 887 (2015); https://doi.org/10.1039/c4fo00790e
[20] H. Korucu, B. Şimşek, A. Yartasi, Arabian Journal for Science and Engineering **43**(11), 6033 (2018); https://doi.org/10.1007/s13369-018-3184-4
[21] H. Korucu, B. Simsek, A. B. Guvenc, V. A. Kucuk, Vibrational Spectroscopy **104**, 102967 (2019); https://doi.org/10.1016/j.vibspec.2019.102967
[22] N. Kumar, S. Das, C. Bernhard, G. D. Varma, Superconductor Science and Technology **26**(9), 095008 (2013); https://doi.org/10.1088/0953-2048/26/9/095008
[23] P. Dakshinamoorthy, S. Vaithilingam, RSC advances **7**(56), 34922 (2017); https://doi.org/10.1039/C7RA04525E
[24] C. H. Manoratne, S. Rosa, I. R. Kottegoda, Material Science Research India, **14**(1), 19 (2017); http://dx.doi.org/10.13005/msri/140104
[25] W. H. Zhang, P. P. He, S. Wu, J. Xu, Y. Li, G. Zhang, X. Y. Wei, Applied Catalysis A: General, **509**, 111 (2016); https://doi.org/10.1016/j.apcata.2015.10.038
[26] J. I. Paredes, S. Villar-Rodil, A. Martínez-Alonso, J. M. Tascon, Langmuir **24**(19), 10560 (2008); https://doi.org/10.1021/la801744a
[27] P. Sehrawat, S. S. Islam, P. Mishra, S. Ahmad, Scientific reports **8**(1), 1 (2018); https://doi.org/10.1038/s41598-018-21686-2
[28] B. Iffath, R. Renjithkumar, T. Devasena, Digest Journal of Nanomaterials and Biostructures **18**(1), 183-193 (2023); https://doi.org/10.15251/DJNB.2023.181.183